PERGAMON

Chemical Engineering Science 54 (1999) 785–802

Chemical Engineering Science

Modelling of the hydrodynamics of the cocurrent gas–liquid trickle flow through a trickle-bed reactor

A. Attou*, C. Boyer, G. Ferschneider

Institut Français du Pétrole, C.E.D.I. René Navarre-Solaize, BP. 3, 69390 Vernaison, France

Received 28 April 1998; accepted 13 October 1998

Abstract

A physical model is developed to predict the hydrodynamic parameters of steady-state cocurrent gas–liquid flow through trickle-bed reactors operating in the trickle flow regime. The trickle flow is described by an annular pattern in which the gas and liquid phases are completely separated by a smooth and stable interface. The formulation of the model involves balance equations deduced from the macroscopic mass and momentum conservation laws. The particle–liquid drag and the gas–liquid interactions, i.e. the gas–liquid drag due to the relative motion between the fluids and the force by which the gas pushes the liquid against the solid particles, are evaluated from theoretical considerations. The predictions of the liquid saturation and pressure gradient from the model are found to be in good agreement with existing experimental data obtained in a wide range of operating pressure (0.1–10 MPa) for various gas–liquid and packing systems. The present model predicts these two hydrodynamic parameters with a better accuracy than the available correlation ones. Some underestimation of the pressure gradient is observed for the highest values of the superficial gas velocity and operating pressure due to the droplets entrainment and the wavy pattern of the gas–liquid interface that are not taken into account. The fundamental feature of the present model is the total absence of adjustable constants.

Keywords: Hydrodynamics; Trickle flow regime; High-pressure trickle-bed reactor; Pressure gradient; Liquid saturation; Phases interactions; Annular pattern

1. Introduction

The trickle-bed reactor is a three-phase catalytic reactor in which a liquid phase and a gas phase flow cocurrently downward through a fixed bed of catalyst solid particles. This reactor is widely used in petrochemical and refinery processes. It provides the flexibility and simplicity of operation as well as high throughputs. The advantage and disadvantages of the trickle-bed reactor are discussed by Satterfield (1975), Gianetto and Specchia (1992) and Saroha and Nigam (1996). The majority of processes occurring in commercial trickle-bed reactors are performed at elevated pressure of up to about 20–30 MPa in order to increase the solubility of the gaseous reactant and achieve better heat transfer.

Several flow regimes exist in a trickle-bed reactor depending on the liquid and gas mass flow rates, the physical properties of the fluids and the geometrical characteristics of the packed bed. Basically four flow regimes can be encountered (Ng, 1986). At low values of the liquid and gas mass flow rates, the liquid trickles over the surface of the packing in the form of rivulets and films and the gas flows in the remaining void volume. This regime is called the trickle flow regime. At higher liquid and gas mass flow rates, a pulsing regime occurs: the liquid blocks the channel between the solid particles and alternate bands of liquid-rich and gas-rich regions traverse the bed. At high gas and low liquid throughputs, the spray regime is observed: the liquid phase is entrained in the form of droplets by the gas phase. In this regime, the gas is the continuous phase. At low gas and high liquid flow rates, the liquid becomes the continuous phase and the gas phase is entrained in the form of bubbles by the liquid phase. This regime is called the dispersed bubble flow regime.

A fundamental understanding of the hydrodynamics of trickle-bed reactors is indispensable in their design,

*Corresponding author. E-mail: abdelouahab.attou@ifp.fr.

0009-2509/99/$ – see front matter
PII: S0009-2509(98)00285-1

scale-up and performance. The hydrodynamics are affected differently in each flow regime (Charpentier and Favier, 1975; Specchia and Baldi, 1977; Rao and Drinkenburg, 1985). Of particular interest in the industry is the extensively used trickle flow encountered at low liquid superficial velocities and low gas superficial velocities. The basic hydrodynamic parameters for the design, scale-up and operation are the pressure gradient and liquid saturation. The pressure gradient is related to the mechanical energy dissipation due to the two-phase flow through the fixed bed of solid particles. It is needed in evaluating the mechanical energy losses, in sizing equipment for pumping and compression of the fluid (Tosun, 1984) and it is used in correlating gas–liquid and liquid–solid mass transfer (Gianetto et al., 1973). The liquid saturation, which partially occupies the void volume of the packed bed, is related to other important hydrodynamic parameters as the pressure gradient, the external wetting of the catalyst particles, the mean residence time of the liquid phase in the reactor and the mass and heat transfer phenomena.

The main objective of this work is to develop a physical model describing the hydrodynamics of the cocurrent gas–liquid trickle flow through a trickle-bed reactor. The trickle flow regime is modelled by an annular flow in which the gas and liquid phases are separated by a smooth and stable interface. Attention is paid to the formulation of the model on the basis of the fundamental macroscopic mass and linear momentum balance equations applied to each phase flow. Furthermore, the formulation of the mutual interactions between the three phases is investigated. The resulting model has no adjusted parameter. The predictions of the pressure gradient and liquid saturation are compared with experimental data of the literature obtained in a wide range of operating pressures. The potentialities of the model to predict the various hydrodynamic phenomena in trickle-bed reactors will be finally discussed.

2. Literature survey

In the literature, a large number of studies have been presented on the various hydrodynamic aspects of trickle-bed reactors. Unfortunately, these research works have been performed at atmospheric pressure in contrast to the industrial trickle-bed reactors which operate at elevated pressures. These studies have led up to the development of several correlations and models of pressure gradient and liquid saturation. The correlations and models that have been established on the basis of atmospheric data are summarised in the articles of Sai and Varma (1987), Ellman et al. (1988,1991), Holub et al. (1993) and Saroha and Nigam (1996).

Recently, some investigations have been performed in pressurised trickle-bed reactors (Hasseni et al., 1987; Ellman et al., 1988, 1991; Wammes and Westerterp, 1990; Wammes et al., 1991a–c; Larachi, 1991a, b; Al-Dahhan and Dudukovic, 1994). The essential results of these works have been summarised in the review article of Al-Dahhan et al. (1997). These studies have shown that the hydrodynamic parameters are considerably affected by the gas density, and the correlations and models based on data at atmospheric pressure are not valid in the whole range of operating pressure. The empirical correlations and model for the prediction of pressure gradient and liquid saturation, that were established on the basis of experimental data obtained in a wide range of operating pressure (around 0.1–10 MPa), are summarised in Table 1 and are pertinent to this study.

On the basis of a dimensional analysis, Ellman et al. (1988, 1991) have derived correlations of pressure gradient and dynamic liquid saturation involving a modified Lockhart–Martinelli parameter, a Reynolds number and a Weber number for the liquid phase. These correlations involve many parameters adjusted to fit two-phase flow data. For the prediction of pressure gradient, the correlation of Ellman et al. (1988) uses four adjusted parameters. On the basis of the same approach, Larachi et al. (1991a, b) have established more simple correlations of pressure gradient and total liquid saturation which can be applied for all regimes. The correlation of Larachi et al. for the prediction of pressure gradient involves five parameters adjusted to fit two-phase flow data. In the works of Ellman et al. (1988, 1991) and Larachi et al. (1991a, b), the pressure gradient and the liquid saturation are correlated separately but it is well known that these two parameters are mutually dependant because they appear simultaneously in the forces balance of each fluid. This is the reason why Wammes et al. (1991b, c) have suggested the use of a set of two correlations in order to predict simultaneously the pressure drop and the dynamic liquid saturation. This set of correlations, established in the trickle flow regime, involves six parameters adjusted to fit two-phase flow data. In order to take into account the gas inertia, Wammes et al. have used a Reynolds number for the gas phase. This choice remains difficult to justify because the gas viscosity effect has not been detected experimentally as this variable is virtually independent of pressure and increases only slightly with increasing temperature.

Al-Dahhan and Dudukovik (1994) have validated the phenomenological model of Holub et al. (1992) based on their experimental data of pressure gradient and liquid saturation obtained in the range of pressure of about 0.31–5 MPa. Holub et al. (1992, 1993) have assumed that the complex geometry of the actual void space in a packed bed can be represented by a single flat slit. The resulting pressure drop and liquid saturation model of Holub et al. is identical to the model of Sweeney (1967) and indicates zero shear stress at the gas–liquid interface. This result implies that the gas flow does not influence

Table 1
Recent correlations based on data obtained in a large range of operating pressure and Holub et al.'s (1992, 1993) model: predictions of the pressure gradient and liquid saturation in trickle-bed reactors operating in the trickle-flow regime

Authors	Pressure	Approach
Ellman et al. (1988, 1991)	0.1–10 MPa	Empirical

$$\frac{(\Delta p/\Delta z)d_h\rho_G}{2G^2} = 200(X_G\delta)^{-1.2} + 85(X_G\delta)^{-0.5}$$

$$\beta_{dyn} = 10^k$$

$$k = 0.001 - \frac{0.42}{\left(X_L^{0.5}\,Re_L^{-0.3}\left(\frac{a_s d_h}{(1-\varepsilon)}\right)^{0.3}\right)^{0.48}}$$

$$\delta = \frac{Re_L^2}{(0.001 + Re_L^{1.5})},\ X_G = \frac{G_G}{G_L}\sqrt{\frac{\rho_L}{\rho_G}},\ X_L = \frac{1}{X_G},\ Re_L = \frac{\rho_L j_L d_p}{\mu_L},$$

where

$$a_s = \frac{6(1-\varepsilon)}{d_p},\ We_L = \frac{G_L^2 d_p}{\rho_L\sigma_L},\ We_G = \frac{G_G^2 d_p}{\rho_G\sigma_L},\ d_h = \left(\frac{16\varepsilon^3}{9\pi(1-\varepsilon)^2}\right)^{0.33} d_p$$

Wammes et al. (1991b, c)	0.2–7.5 MPa	Empirical

$$\frac{(\Delta p/\Delta z)d_p}{\frac{1}{2}\rho_G j_G^2} = 155\left(\frac{\rho_G j_G d_p \varepsilon}{\mu_G(1-\varepsilon)}\right)^{-0.37}\left(\frac{1-\varepsilon}{\varepsilon(1-\beta_{tot})}\right)$$

$$\beta_{dyn} = 3.8\left(\frac{\rho_L j_L d_p}{\mu_L}\right)^{0.55}\left(\frac{d_p^3\rho_L^2 g}{\mu_L^2}\left(1 + \frac{\Delta p/\Delta z}{\rho_L g}\right)\right)^{-0.42}\left(\frac{6(1-\varepsilon)d_p}{\varepsilon}\right)^{0.65}$$

Larachi et al. (1991)	0.2–8.1 MPa	Empirical

$$\frac{(\Delta p/\Delta z)d_h\rho_G}{2G_G^2} = \frac{1}{((Re_L We_L)^{0.25}X_G)^{1.5}}\left(31.3 + \frac{17.3}{((Re_L We_L)^{0.25}X_G)^{1.5}}\right)$$

$$\beta_{tot} = 1 - 10^{-\Gamma}$$

$$\Gamma = 1.22\frac{We_L^{0.15}}{X_G^{0.15}Re_L^{0.2}}$$

where the definitions of X_G, Re_L, We_L and d_h are the same as Ellman et al.'s correlation ones

Holub et al. (1992, 1993) Al-Dahhan and Dudukovic (1994)	0.31–5 MPa	Phenomenological

$$\Psi_L = \frac{\Delta p/\Delta z}{\rho_L g} + 1 = \left(\frac{1}{\beta_{tot}}\right)^3\left(\frac{E_1 Re_L}{Ga_L} + \frac{E_2 Re_L^2}{Ga_L}\right)$$

$$\Psi_G = \frac{\Delta p/\Delta z}{\rho_G g} + 1 = \left(\frac{1}{1-\beta_{tot}}\right)^3\left(\frac{E_1 Re_G}{Ga_G} + \frac{E_2 Re_G^2}{Ga_G}\right)$$

$$\Psi_L = 1 + \frac{\rho_G}{\rho_L}(\Psi_G - 1)$$

where $Re_K = \dfrac{\rho_K j_K d_p}{\mu_K(1-\varepsilon)}$, $Ga_K = \dfrac{\rho_K^2 d_p^3 g\varepsilon^3}{\mu_K^2(1-\varepsilon)^3}$ $(K = L \text{ or } G)$

and E_1 and E_2 are parameters to be determined from single-phase flow experiments

the liquid flow. However, the experimental studies of Wammes and Westerterp (1990), Wammes et al. (1991a–c), Larachi (1991), Larachi et al. (1991a, b, 1994) and Al-Dahhan and Dudukovic (1994) have shown that the gas flow has a considerable influence on the hydrodynamics of the trickle-bed reactor especially at high operating pressures. Accordingly, the interactions between the gas and liquid phases are not negligible with regard to the other momentum transfer mechanisms. This means that the model of Holub et al. (1992) is based on an assumption which is not satisfied in the whole range of operating conditions especially at elevated pressures. Moreover, the model of Holub et al. involves two parameters adjusted to fit single-phase flow data.

Each empirical correlation has been established on the basis of a data set obtained in a specific range of operating conditions, fluid properties and bed characteristics. They involve several parameters adjusted to fit two-phase flow data. These parameters are not universal constants. Moreover, these correlations have no physical basis and do not allow a better understanding of hydrodynamic phenomena in trickle-bed reactors. The predicted values of pressure gradient and liquid saturation from these three correlations vary too much. Thus their reliability for use in the design, scale-up and operation of industrial trickle-bed reactors may be discussed. On the other hand, the model of Holub et al. (1992) does not take into account the mutual interactions between the gas and liquid phases. These fundamental interactions are the origin of several important hydrodynamic phenomena experimentally observed in trickle-bed reactors. Moreover, this model needs a preliminary determination of the two parameters from single-phase flow experiments. Unfortunately, these kind of experiments is difficult or impossible to perform in the industrial practice. These aspects reduce considerably the potentiality of this model.

3. Basic assumptions and idealisation of the trickling flow

A two-phase two-component cocurrent gas–liquid trickle flow through a fixed bed of solid particles is considered. The one-dimensional fully established two-phase flow is steady-state and isothermal and both the flowing phases are assumed as Newtonian fluids. As the flow is isothermal, the liquid density does not change significantly. The liquid phase is thus considered as incompressible: $\rho_L = \text{cst}$. The gaseous phase is considered as ideal gas: $\rho_G = p/RT$. The ideal behaviour of the gas phase remains a good approximation for operating conditions not too close to the critical point.

A typical sketch of two-phase trickle flow in an interstitial void volume between particles is represented in Fig. 1. The trickle flow regime can be divide into two regions (Ng and Chu, 1987). At very low gas and liquid

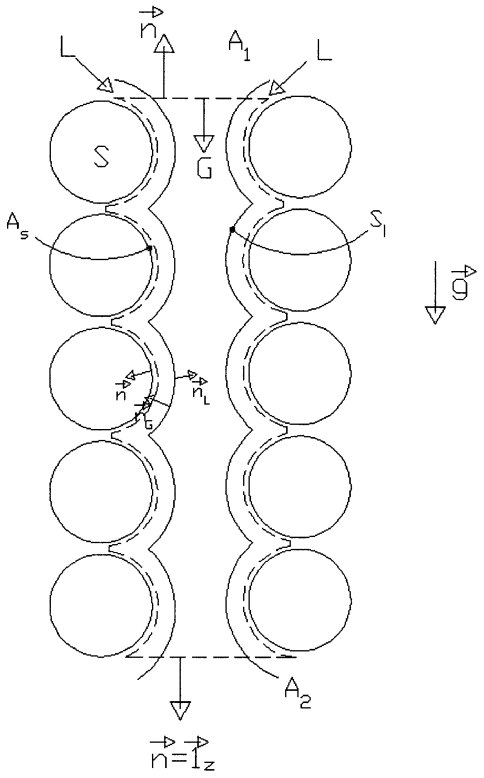

Fig. 1. Schematic representation of the cocurrent gas–liquid downward flow through the interstitial void space of the packed bed.

flow rates, a fraction of the packing surface remains unwetted. When the liquid flow rate is increased, the partial wetting regime changes to complete wetting regime in which the total packing surface is covered by a liquid film. This last situation is more plausible because the industrial trickle-bed reactors often operate in regions close to the transition from trickling to pulsing flow (Satterfield, 1975). Accordingly, the packing surface is assumed totally covered by a liquid film and the gas flows in the central zone of the interstitial void volume (Fig. 1). On the basis of this idealisation of the trickle flow regime, the two-phase flow can be assumed to be an annular flow in which the gas and liquid phases are completely separated by a smooth and stable interface. Each fluid behaves as a continuous medium for which the macroscopic balance equations may be expressed according to the eulerian formalism.

On the other hand, the hydrodynamic variables are assumed uniform over the whole cross-sectional area of the trickle-bed reactor: the effects of global non-uniformity of the flow distribution in the packed bed are neglected. The flow variables in the elementary interstitial void volume are considered as representative of the respective averaged variables over the cross-sectional area of the reactor.

4. Formulation of the trickle flow model

4.1. Control volume

Let a control volume V of the interstitial void space, which does not vary with time, bounded by the closed surface S defined by (Fig. 1):

$$S = A_1 \cup A_S \cup A_2$$

where A_1 and A_2 represent the inlet and outlet geometrical cross-sections and A_S is the solid particles wall area. The control volume is assumed to include enough particles to smooth the local fluctuations of the hydrodynamic variables and to keep only the macroscopic variations of their averaged values.

The macroscopic conservation laws are applied to the fraction of control volume occupied on average by the K-fluid ($K = G$ or L).

4.2. Mass balance equation of each fluid phase

The mass balance equation for K-fluid can be written in the form:

$$\int_{A_S} \bar{\mathbf{X}}_K \rho_K \mathbf{v}_K \mathbf{n}\, \mathrm{d}S + \int_{A_1} \bar{\mathbf{X}}_K \rho_K \mathbf{v}_K \mathbf{n}\, \mathrm{d}S + \int_{A_2} \bar{\mathbf{X}}_K \rho_K \mathbf{v}_K \mathbf{n}\, \mathrm{d}S + \int_{S_i} \rho_K (\mathbf{v}_K - \mathbf{v}_i) \mathbf{n}\, \mathrm{d}S = 0 \quad (1)$$

where $\mathbf{X}_K$ is the characteristic presence function of the K-phase (0 or 1), $\mathbf{v}_K$ is the velocity of the K-phase, ρ_K is the density of the K-phase, $\mathbf{n}$ is the unit vector normal to S, oriented towards the outside of volume V, $\mathbf{n}_K$ is the unit vector normal to the gas–liquid interface S_i, oriented away from the K-phase, and $\mathbf{v}_i$ is the gas–liquid interface velocity.

For a two-component gas–liquid system, the last term of Eq. (1) characterizing the mass transfer between fluids is zero. For non-porous particles, the packing surface is impermeable. For porous particles the velocity associated to mass transfer across the solid wall remains small compared to the transit velocity of fluids across the interstitial volume. Accordingly, in all cases the first term of Eq. (1) associated to the mass transfer across the solid wall is zero and the mass balance equation for K-phase is reduced to the following form:

$$\int_{A_2} \bar{\mathbf{X}}_K \rho_K \mathbf{v}_K \mathbf{1}_z\, \mathrm{d}S - \int_{A_1} \bar{\mathbf{X}}_K \rho_K \mathbf{v}_K \mathbf{1}_z\, \mathrm{d}S = 0 \quad (2)$$

where $\mathbf{1}_z$ is the unit vector in the axial direction z.

After dividing each member of Eq. (2) by the elementary volume $V = A\,\mathrm{d}z$, where A is the effective cross-sectional area of the interstitial space and $\mathrm{d}z$ is the elementary distance between the cross-sections A_1 and A_2, the following mass balance equations are obtained

for the gas and liquid phases, respectively,

$$\frac{\mathrm{d}}{\mathrm{d}z}(\alpha\rho_G u_G) = 0$$
$$\frac{\mathrm{d}}{\mathrm{d}z}((1-\alpha)\rho_L u_L) = 0 \tag{3}$$

where the axial velocity of the K-phase averaged over the cross-sectional area A_K (u_K) and the fraction of the effective cross-sectional area A occupied on average by the K-phase (α_K) are, respectively, defined by the following expressions:

$$u_K = \frac{1}{A_K}\int_{[A_K]} \mathbf{v}_K \mathbf{1}_z \,\mathrm{d}S \quad \text{and} \quad \alpha_K = \frac{A_K}{A}.$$

According to the theorem of Dupuit, for homogeneous, isotropic and unconsolidated packed beds, the quantities $\alpha = \alpha_G$ and $1-\alpha = \alpha_L$ denote the mean fractions of the interstitial void volume occupied on average by the gas and liquid phases, respectively (theorem of Dupuit). The liquid saturation in the trickle-bed reactor is thus given from $1-\alpha$.

4.3. Linear momentum balance equation of each fluid phase

The linear momentum balance equation of the K-fluid can be written in the form:

$$\oint_S \bar{\mathbf{X}}_K(\rho_K \mathbf{v}_K(\mathbf{v}_K\mathbf{n}) - \mathbf{T}_K.\mathbf{n})\,\mathrm{d}S + \int_{S_i}(\rho_K\mathbf{v}_K(\mathbf{v}_K-\mathbf{v}_i)\mathbf{n}_K - \mathbf{T}_K.\mathbf{n}_K - \tau_i\mathbf{n}_K)\,\mathrm{d}S - \int_{A_S}\bar{\mathbf{X}}_K\tau_i\mathbf{n}\,\mathrm{d}S = \int_V \bar{\mathbf{X}}_K\rho_K\mathbf{g}\,\mathrm{d}V \tag{4}$$

where $\mathbf{T}_K$ is the total stress tensor of K-fluid, $\mathbf{g}$ is the gravitational acceleration and τ_i denotes the interfacial shear stress contributing to the local momentum transfer at the gas–liquid (S_i) and liquid–solid (A_S) material interfaces (Ishii, 1975).

Each flowing fluid is submitted simultaneously to the actions of total stress, inertia and gravity forces. The resultant of total stress forces involves a contribution due to the shear stress exerted at the surface of solid particles and another one due to the mutual interactions between the flowing fluids at the gas–liquid interface.

As there is no mass transfer between the phases, the condition $\rho_K(\mathbf{v}_K-\mathbf{v}_i)\mathbf{n}_K = 0$ is satisfied on the gas–liquid interface S_i and thus the projection of the vectorial equation (4) along the axial direction z gives:

$$\begin{aligned}&\int_{A_2}\bar{\mathbf{X}}_K(\rho_K(\mathbf{v}_K\mathbf{1}_z)^2 + p_K)\,\mathrm{d}S - \int_{A_1}\bar{\mathbf{X}}_K(\rho_K(\mathbf{v}_K\mathbf{1}_z)^2 + p_K)\,\mathrm{d}S \\ &+ \int_{A_1}\bar{\mathbf{X}}_K\tau_{K,zz}\,\mathrm{d}S - \int_{A_2}\bar{\mathbf{X}}_K\tau_{K,zz}\,\mathrm{d}S - \int_{A_S}\bar{\mathbf{X}}_K\tau_{K,nz}\,\mathrm{d}S - \int_{S_i}\tau_{K,nz}\,\mathrm{d}S \\ &- \int_{A_S}\bar{\mathbf{X}}_K\tau_i(\mathbf{n}_K\mathbf{1}_z)\,\mathrm{d}S - \int_{S_i}\tau_i(\mathbf{n}_K\mathbf{1}_z)\,\mathrm{d}S \\ &+ \int_{A_S\cup S_i}\bar{\mathbf{X}}_K p_K(\mathbf{n}_K\mathbf{1}_z)\,\mathrm{d}S = \int_V \bar{\mathbf{X}}_K\rho_K\, g\,\mathrm{d}V\end{aligned} \tag{5}$$

where the total stress tensor of the K-fluid has been decomposed into the scalar tensor proportional to the pressure p_K and the viscous stress tensor $\boldsymbol{\tau}_K$ for the K-fluid:

$$\mathbf{T}_K = -p_K\mathbf{I} + \boldsymbol{\tau}_K.$$

The components of the viscous stress tensor for the K-fluid $\tau_{K,zz}$ and $\tau_{K,nz}$ are defined, respectively, by

$$\tau_{K,zz} = \mathbf{1}_z(\boldsymbol{\tau}_K\mathbf{1}_z) \quad \text{and} \quad \tau_{K,nz} = \mathbf{1}_z(\boldsymbol{\tau}_K\mathbf{n}).$$

As each flowing phase is assumed to be a Newtonian viscous fluid, the longitudinal component of the viscous stress tensor can be expressed in the form:

$$\tau_{K,zz} = 2\mu_K\frac{\mathrm{d}u_K}{\mathrm{d}z}$$

where μ_K is the dynamic viscosity of the K-fluid. As a consequence, the resultant of longitudinal viscous stress forces is several orders of magnitude smaller than the resultant of pressure forces exerted at the cross-sectional areas A_1 and A_2. Thus these terms can be neglected in Eq. (5) which becomes:

$$\begin{aligned}&\int_{A_2}\bar{\mathbf{X}}_K(\rho_K(\mathbf{v}_K\mathbf{1}_z)^2 + p_K)\,\mathrm{d}S - \int_{A_1}\bar{\mathbf{X}}_K(\rho_K(\mathbf{v}_K\mathbf{1}_z)^2 + p_K)\,\mathrm{d}S \\ &- \int_{A_S}\bar{\mathbf{X}}_K\tau_{K,nz}\,\mathrm{d}S - \int_{S_i}\tau_{K,nz}\,\mathrm{d}S \\ &- \int_{A_S}\bar{\mathbf{X}}_K\tau_i(\mathbf{n}_K\mathbf{1}_z)\,\mathrm{d}S - \int_{S_i}\tau_i(\mathbf{n}_K\mathbf{1}_z)\,\mathrm{d}S \\ &+ \int_{A_S\cup S_i}\bar{\mathbf{X}}_K p_k(\mathbf{n}_K\mathbf{1}_z)\,\mathrm{d}S = \int_V \bar{\mathbf{X}}_K\rho_K g\,\mathrm{d}V.\end{aligned} \tag{6}$$

The axial momentum balance equations for the gas and liquid phases result from the division of each member of Eq. (6) by the volume $V = A\,\mathrm{d}z$ of the interstitial void space. It is noted that an additional relation between the two-phase pressures p_G and p_L is needed. In principle, this

relation can be deduced from a linear momentum balance expressed at the vicinity of the gas–liquid interface. Unfortunately, it is difficult to exploit this approach due to the complexity of the interface geometry and local transfer phenomena. Several authors have used the representation of the capillary pressure $p_C = p_G - p_L$ by the Leverett's function which has found extensive use in the analysis of multiphase flow through porous media to provide a relation between p_G and p_L (Saez and Carbonell, 1985; Grosser et al., 1988; Dankworth et al., 1990). However, the validity of such a representation for trickle-bed reactors has not been established. This representation implies that the capillary pressure gradient is proportional to the gradient of the liquid fraction $(1-\alpha)$. As the liquid fraction does not change significantly with z for a steady-state fully established flow, the capillary pressure gradient $\mathrm{d}p_C/\mathrm{d}z$ can be neglected with regard to the fluid pressure gradient $\mathrm{d}p_K/\mathrm{d}z$:

$$\frac{\mathrm{d}p_G}{\mathrm{d}z} = \frac{\mathrm{d}p_L}{\mathrm{d}z} = \frac{\mathrm{d}p}{\mathrm{d}z}.$$

This approximation is acceptable for the modelling of the steady-state macroscopic average hydrodynamic bed behaviour because usually only a small fraction of the reactor volume is submitted to the capillary effects. By taking into account this approximation and the following equalities:

$$-\int_{A_S \cup S_i} \bar{\mathbf{X}}_K p_K (\mathbf{n}_K \mathbf{1}_z) \frac{\mathrm{d}S}{A\,\mathrm{d}z} = p_K \frac{1}{A}\frac{\mathrm{d}A_K}{\mathrm{d}z} = p_K \frac{\mathrm{d}\alpha_K}{\mathrm{d}z}$$

the axial momentum balance equations for respectively the gas and liquid phases can be written as follows:

$$\alpha \frac{\mathrm{d}p}{\mathrm{d}z} = -\Gamma_G \frac{\mathrm{d}}{\mathrm{d}z}(\alpha \rho_G u_G^2) + f_{\mathrm{int},G} + \alpha \rho_G g$$

$$(1-\alpha)\frac{\mathrm{d}p}{\mathrm{d}z} = -\Gamma_L \frac{\mathrm{d}}{\mathrm{d}z}((1-\alpha)\rho_L u_L^2) + f_{\mathrm{int},L} + (1-\alpha)\rho_L g \qquad (7)$$

where the shape factor Γ_K is defined by the relation:

$$\Gamma_K = \frac{1}{A_K u_K^2}\int_{(A_K)} (\mathbf{v}_K \mathbf{1}_z)^2\,\mathrm{d}S$$

and the resultant of interaction forces exerted on the K-fluid per unit volume of the void space in the packed bed, $f_{\mathrm{int},K}$, is defined by the integral expression:

$$f_{\mathrm{int},K} = \frac{1}{V}\int_{A_S} \bar{\mathbf{X}}_K(-\tau_{K,nz})\,\mathrm{d}S + \frac{1}{V}\int_{S_i}(-\tau_{K,nz})\,\mathrm{d}S + \frac{1}{V}\int_{A_S} \bar{\mathbf{X}}_K \tau_i(-\mathbf{n}_K \mathbf{1}_z)\,\mathrm{d}S + \frac{1}{V}\int_{S_i}\tau_i(-\mathbf{n}_K \mathbf{1}_z)\,\mathrm{d}S.$$

The shape factor Γ_L which characterises the liquid film velocity has a similar definition to the shape parameter defined by Hanratty (1983) and Malamatenios et al. (1994) in their two-phase layer–liquid film model. For a laminar liquid film, calculations of the boundary layer show that the value of Γ_L is 4/3. For a fully turbulent gas flow, the value of Γ_G can be assumed equal to 1 due to the fact that the gas velocity profile is usually flat over the cross-sectional area of the interstitial void volume.

This approach shows that the one-dimensional mass and linear momentum balance formulations for each fluid (sets (3) and (7)) can be established by applying the macroscopic balance equations to the part of interstitial void volume occupied on average by the gas or liquid phase. The set of equations (3) and (7) constitutes a separated-phase model of the gas–liquid trickling flow that will be called the *trickle flow model*. In order to solve the set of equations (3) and (7), closure equations for the interactions between phases ($f_{\mathrm{int},G}$ and $f_{\mathrm{int},L}$) must be established.

5. Closure equations for the hydrodynamic interactions

5.1. Hydrodynamic interactions balances

A schematic representation of the hydrodynamic interactions in the three-phase system is shown in Fig. 2. As the external area of solid particles is assumed totally covered by a liquid film, the gas flow does not exert a direct action on the packing surface ($\bar{\mathbf{X}}_G = 0$ on A_S). Accordingly, the resultant of interaction forces exerted on the gas phase is only induced by effects located at the gas–liquid interface:

$$f_{\mathrm{int},G} = \frac{1}{V}\int_{S_i}(-\tau_{G,nz})\,\mathrm{d}S + \frac{1}{V}\int_{S_i}\tau_i(-\mathbf{n}_G \mathbf{1}_z)\,\mathrm{d}S \qquad (8a)$$

The interfacial force $f_{\mathrm{int},G}$ exerted on the gas phase involves two components. The first component in Eq. (8a) is the drag force $-f_{GL}$ exerted on the gas phase due to the relative motion between the two fluids. This drag

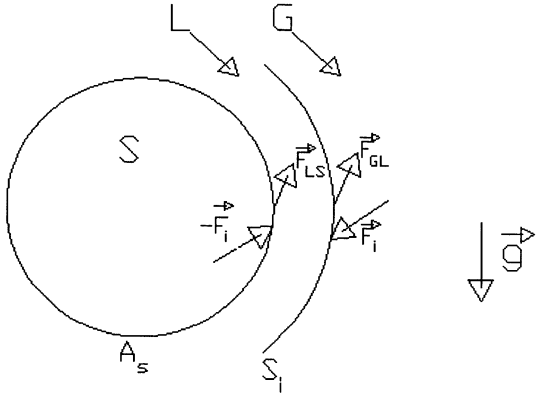

Fig. 2. Schematic representation of the interactions forces in the three-phase system.

force is resulting from the shear stress τ_G exerted on the gaseous boundary layer located at the vicinity of the gas–liquid interface. It is opposed to the slip between the flowing phases. The second component in Eq. (8a) is the force opposed to the gas motion which is exerted on the gas phase resulting from the shear stress τ_i of the material interface between the fluids. It is noted that this force vanishes if the gas–liquid interface is perfectly flat and vertical ($\mathbf{n}_G . \mathbf{1}_z = 0$). Thus the term $(1/V)\int_{S_i} \tau_i(\mathbf{n}_G \mathbf{1}_z)\,\mathrm{d}S = f_i$ is interpreted as the fraction of the gas momentum which is transferred to the packing surface across the liquid film due to the tortuous pattern and the successive cross-sectional area changes of the interstitial flow path. This momentum transfer can be viewed as an interfacial force f_i by which the gas pushes on solid particles through the liquid layer. Consequently, the resultant of the interaction forces exerted on the gas phase per unit volume of void space can be written as follows:

$$f_{\mathrm{int},G} = -(f_{GL} + f_i). \tag{8b}$$

As the area of solid particles is totally wetted by a liquid film ($\bar{\mathbf{X}}_L = 1$ on A_S), the liquid flow exerts a direct action on the packing surface. Accordingly, the resultant of interaction forces exerted on the liquid phase is contributed by effects located at the liquid–solid as well as gas–liquid interfaces:

$$f_{\mathrm{int},L} = \frac{1}{V}\int_{A_S} (-\tau_{L,nz})\,\mathrm{d}S + \frac{1}{V}\int_{S_i} (-\tau_{L,nz})\,\mathrm{d}S + \frac{1}{V}\int_{A_S} \tau_i(-\mathbf{n}_L \mathbf{1}_z)\,\mathrm{d}S + \frac{1}{V}\int_{S_i} \tau_i(-\mathbf{n}_L \mathbf{1}_z)\,\mathrm{d}S \tag{9a}$$

On the basis of the mechanical principle action equal reaction, the term $(1/V)\int_{A_S} \tau_i(-\mathbf{n}_L \mathbf{1}_z)\,\mathrm{d}S$ of Eq. (9a) represents the reaction exerted on the liquid layer by the fixed solid particles which is equal and opposed to the force f_i given by $(1/V)\int_{S_i} \tau_i(-\mathbf{n}_L \mathbf{1}_z)\,\mathrm{d}S$. Thus the Eq. (9a) is reduced to the following form:

$$f_{\mathrm{int},L} = \frac{1}{V}\int_{A_S} (-\tau_{L,nz})\,\mathrm{d}S + \frac{1}{V}\int_{S_i} (-\tau_{L,nz})\,\mathrm{d}S \tag{9b}$$

It can be noted that the force by which the gas phase pushes the liquid film against the solid particles, produced by the tortuous pattern and the cross-sectional area-changes of the flow path, does not appear in the above expression of the resultant $f_{\mathrm{int},L}$. That is because this force is added to the reaction equal and opposed exerted by the packing surface on the liquid film to give zero.

The first component in Eq. (9b) is the drag force $-f_{LS}$ exerted on the liquid phase due to the shear stress τ_L in the liquid boundary layer located at the vicinity of the packing surface. This force is opposed to the liquid motion. On the other hand, it can be shown from the balance law of momentum transfer at the gas–liquid interface

$$\frac{1}{V}\int_{S_i} (-\tau_{L,nz})\,\mathrm{d}S = \frac{1}{V}\int_{S_i} \tau_{G,nz}\,\mathrm{d}S = f_{GL}$$

that the second component in Eq. (9b) is the gas–liquid drag force f_{GL} resulting from the slip motion between the fluids. Consequently, the resultant of the interaction forces exerted on the liquid phase per unit volume of void space can be written as follows:

$$f_{\mathrm{int},L} = f_{GL} - f_{LS}. \tag{9c}$$

5.2. Single-phase gas flow

Each component of the interaction term $f_{\mathrm{int},K}$ involves a viscous contribution proportional to the quantity $\mu_K v_K$ and another one due to the fluid inertia $\rho_K v_K^2$. The theoretical formulation which takes into account this aspect is the Kozeny–Carman's equation. This equation has a fundamental basis since it arises from a momentum balance applied to the single-phase gas flow through an assumed pore geometry. The equation of Kozeny–Carman gives for a single-phase gas flow the particle–gas drag force f per unit volume of void space in the packed bed:

$$f = A\mu_G j_G + B\rho_G j_G^2 \tag{10}$$

where j_G is the superficial velocity of the gas phase based on the total cross-sectional area of the reactor, and the parameters A and B, function of geometrical characteristics of the packed bed, are defined, respectively, by the relations:

$$A = 180\frac{(1-\varepsilon)^2}{\varepsilon^3 d_p^2} \quad \text{and} \quad B = 1.8\frac{(1-\varepsilon)}{\varepsilon^3 d_p}$$

where ε is the global porosity of the packed bed and d_p is the equivalent diameter of the particles ($d_p = 6\,V_p/S_p$ where V_p and S_p are the volume and the area of a particle, respectively).

The numerical values 180 and 1.8 have been recommended by Mc Donald et al. (1979). These authors have compared the predictions given from Eq. (10) with several experimental data of the literature obtained for single-phase flow through packed beds of various geometrical characteristics. They have concluded that the functional dependence of the Kozeny–Carman's equation correctly represents the experimental data. The numerical constants 180 and 1.8 have been used by other researchers as Saez and Carbonell (1985) and Grosser et al. (1988).

5.3. Two-phase gas–liquid flow

Since the gas and liquid phases are assumed completely separated by a smooth and stable interface and each fluid behaves as a continuous medium, the

Kozeni–Carman's equation can be applied to each fluid as long as the assumed two-phase trickling pattern is correctly taken into account.

By taking into consideration the physical properties and the superficial velocity of the liquid, the liquid–solid drag force per unit volume of void space is found to be proportional to $(A_{LS}\mu_L j_L + B_{LS}\rho_L j_L^2)$ where A_{LS} and B_{LS} are the liquid–solid momentum transfer coefficients. This quantity must be multiplied by $(1-\alpha)$ in order to take into account the volume fraction of void space occupied on an average by the liquid phase:

$$f_{LS} = (1-\alpha)(A_{LS}\mu_L j_L + B_{LS}\rho_L j_L^2)\,\theta_L(\alpha) \tag{11a}$$

where $\theta_L > 1$ is a factor taking into account the average tortuous pattern of the liquid films at the macroscopic level. This factor is defined as the ratio of the average length of interstitial flow paths over the height of the reactor. When the liquid volume fraction increases, the tortuous pattern factor θ_L decreases due to the higher inertia of the liquid phase with respect to the hydrodynamic resistance of the packed bed. Accordingly, the average tortuous pattern factor is assumed to be inversely proportional to the liquid volume fraction and function only of $1-\alpha$:

$$\theta_L(\alpha) = \frac{1}{1-\alpha}. \tag{11b}$$

By taking into account expressions (11a) and (11b), the liquid–solid drag force per unit volume of void space is given from the equation:

$$f_{LS} = A_{LS}\mu_L j_L + B_{LS}\rho_L j_L^2. \tag{11c}$$

It can be noted from the resulting relation (11c) that approximation (11b) implies that the liquid films on an average have access by dribbling to the total open cross-section of the packed-bed reactor. This assumption remains physically consistent with the highly tortuous flow paths of liquid films and rivulets experimentally observed in the trickle flow regime even for conditions of elevated gas and liquid throughputs.

As the packing surface is totally covered by a liquid film, the particle diameter and the volume fraction of the solid catalyst which participate in the liquid–solid drag phenomenon are respectively d_p and $(1-\varepsilon)$. However, the volume fraction of liquid which contributes to the liquid–solid drag is not given by the void fraction ε of the packed bed (as it was the case for the single-phase gas flow) but it is equal to $(1-\alpha)\varepsilon$. By taking into account these aspects, the liquid–solid momentum transfer coefficients are expressed by

$$A_{LS} = 180\,\frac{(1-\varepsilon)^2}{(1-\alpha)^3\varepsilon^3 d_p^2} \quad \text{and} \quad B_{LS} = 1.8\,\frac{(1-\varepsilon)}{(1-\alpha)^3\varepsilon^3 d_p}. \tag{11d}$$

By taking into consideration the physical properties of the gas phase and a reference superficial velocity j_r associated with the relative motion of fluids, the gas–liquid drag force per unit volume of void space is found to be proportional to $(A_{GL}\mu_G j_r + B_{GL}\rho_G j_r^2)$ where A_{GL} and B_{GL} are the gas–liquid momentum transfer coefficients. This quantity must be multiplied by α in order to take into account the volume fraction of void space occupied on an average by the gas phase. Accordingly, the gas–liquid drag force per unit volume of void space is given from the equation:

$$f_{GL} = \alpha(A_{GL}\mu_G j_r + B_{GL}\rho_G j_r^2) \tag{12a}$$

The effects of slip between the gas and liquid phases are taken into account by considering the following reference superficial velocity:

$$j_r = j_G - \left(\frac{\alpha}{1-\alpha}\right) j_L \tag{12b}$$

which represents well the gas–liquid relative motion for the two-phase annular flow pattern.

Due to the presence of the liquid film, the gas flows across particles having an effective diameter greater than the actual diameter of solid particles d_p. The geometrical correction taking into account the increase of the particle volume due to the liquid layer leads to an effective diameter equal to $((1-\alpha\varepsilon)/(1-\varepsilon))^{1/3}\,d_p$. On the other hand, the bed of particles covered by the liquid layer can be interpreted for the gas flow as a packed bed for which the effective global porosity is smaller than the global porosity of the actual bed ε. The correction taking into account the presence of the liquid film leads to an effective global porosity for the gas flow equal to $\alpha\varepsilon$. According to these aspects, the gas–liquid momentum transfer coefficients are expressed by

$$A_{GL} = 180\,\frac{(1-\alpha\varepsilon)^2}{\alpha^3\varepsilon^3 d_p^2}\left(\frac{1-\varepsilon}{1-\varepsilon\alpha}\right)^{2/3} \quad \text{and}$$

$$B_{GL} = 1.8\,\frac{(1-\alpha\varepsilon)}{\alpha^3\varepsilon^3 d_p}\left(\frac{1-\varepsilon}{1-\alpha\varepsilon}\right)^{1/3}. \tag{12c}$$

Finally, by taking into consideration the physical properties and the superficial velocity of the gas phase, the force by which the gas pushes on the solid particles per unit volume of void space is found to be proportional to $(A_i\mu_G j_G + B_i\rho_G j_G^2)$ where A_i and B_i are interfacial momentum transfer coefficients. This quantity must be multiplied by the volume fraction of void space occupied on an average by the gas phase α. Accordingly, the interfacial force per unit volume of void space is given by the equation:

$$f_i = \alpha(A_i\mu_G j_G + B_i\rho_G j_G^2). \tag{13a}$$

On the basis of a reasoning similar to that for the gas–liquid interaction, the following equations are obtained:

$$A_i = A_{GL} \quad \text{and} \quad B_i = B_{GL}. \tag{13b}$$

6. Resulting trickle flow model

By taking into account sets (3) and (7) and Eq. (11c), (12a), (13a) and (13b), the hydrodynamic trickle flow model can be written in the following form:

$$\frac{1}{p}\frac{\mathrm{d}p}{\mathrm{d}z} + \frac{1}{\alpha}\frac{\mathrm{d}\alpha}{\mathrm{d}z} + \frac{1}{u_G}\frac{\mathrm{d}u_G}{\mathrm{d}z} = 0$$

$$\frac{1}{1-\alpha}\frac{\mathrm{d}(1-\alpha)}{\mathrm{d}z} + \frac{1}{u_L}\frac{\mathrm{d}u_L}{\mathrm{d}z} = 0$$

$$\alpha\frac{\mathrm{d}p}{\mathrm{d}z} = -\frac{\Gamma_G}{RT}\alpha p u_G\frac{\mathrm{d}u_G}{\mathrm{d}z} - \alpha(A_{GL}(\alpha)\mu_G(j_r + j_G) + B_{GL}(\alpha)\rho_G(j_r^2 + j_G^2)) + \alpha\rho_G g \tag{14}$$

$$(1-\alpha)\frac{\mathrm{d}p}{\mathrm{d}z} = -\Gamma_L(1-\alpha)\rho_L u_L\frac{\mathrm{d}u_L}{\mathrm{d}z} + \alpha(A_{GL}(\alpha)\mu_G j_r + B_{GL}(\alpha)\rho_G j_r^2) - (A_{LS}(\alpha)\mu_L j_L + B_{LS}(\alpha)\rho_L j_L^2) + (1-\alpha)\rho_L g$$

where the coefficients $A_{KK'}(\alpha)$ and $B_{KK'}(\alpha)$, function of gas fraction α and geometrical characteristics of the packed bed (ε, d_p), are calculated from expressions (11d) and (12c).

The trickle flow model (14) involves four equations with four variables (α, u_G, u_L and p). For given operating conditions (superficial velocity of each fluid, operating pressure and temperature), fluids properties and packed bed characteristics, the hydrodynamic model (14) is integrated step by step starting from the inlet up to the outlet of the trickle-bed reactor by means of the fourth-order Runge–Kutta algorithm. Single-phase liquid and two-phase gas–liquid flow runs have been performed over a range of operating conditions spanning the trickling flow regime. A summary of the experimental data of the literature gathered in this study is presented in Table 2. The hydrodynamic parameters measured by the authors, i.e. the pressure gradient and the liquid saturation, are obtained in a wide range of operating pressure (about 0.1–10 MPa) and for various gas–solid–liquid systems.

7. Results

7.1. Single-phase liquid trickle flow

A particular case of the two-phase trickle flow model (14) is liquid film flow in a stagnant gas ($j_G = 0$). Without gas flow, no shear stress is exerted on the liquid film by the gas phase and flow is only due to gravity with a resistance due to the shear stress at the liquid–solid interface. In these conditions, Wammes et al. (1991a) have measured the dynamic liquid saturation β_{dyn} for various liquids and operating pressures. The dynamic liquid saturation is calculated from the present model by the relation: $\beta_{dyn} = 1 - \alpha - \beta_{stat}$ where the static liquid saturation β_{stat} has been determined experimentally by the authors.

Fig. 3 compares the experimental data of Wammes et al. (1991a) with the calculated results of the present model. The numerical results are satisfactorily close to the experimental ones in the whole range of liquid Reynolds number. The relative error (the absolute difference between the experimental and predicted values divided by the experimental value) is equal on average to about 10%. The comparison of the curves related to water (aqueous liquid) and ethyleneglycol (organic viscous liquid) shows that the sensitivity of the model to changes in liquid viscosity is good: the dynamic liquid saturation increases with the liquid viscosity. For liquids of high viscosity, the shear stress at the liquid–solid interface is of importance compared to the gravity force and accordingly the mean residence time of liquid in the reactor becomes more significant. Furthermore, the comparison of curves obtained for water shows that the theoretical simulations predict correctly the very small influence of operating pressure. This was to be expected since the liquid phase is assumed to be incompressible in the model.

7.2. Two-phase gas–liquid trickle flow

Wammes et al. (1990, 1991a–c) have performed measurements of pressure gradient and dynamic liquid

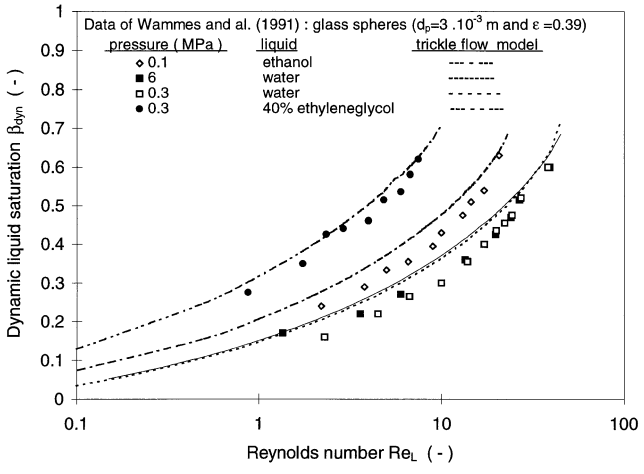

Fig. 3. Dynamic liquid saturation vs the liquid Reynolds number in the conditions of single-phase liquid trickle flow ($j_G = 0$): comparison of the theoretical predictions from the trickle flow model with the experimental results of Wammes et al. (1991a).

saturation for cocurrent gas–liquid trickle flows through packed beds of glass beads and ceramic cylinders in the range of operating pressure 0.2–7.5 MPa. At a value of operating pressure equal to 6 MPa and with two different gases (helium and nitrogen), the predictions of the present model are compared with experimental results of Wammes et al. in Figs. 4 and 5 for pressure gradient and dynamic liquid saturation, respectively. The model predicts correctly the trends experimentally observed. At a given gas density the pressure gradient increases with the superficial fluids velocities; and at given superficial velocities it increases with gas density (via the operating pressure or/and the gas molecular weight). Additionally,

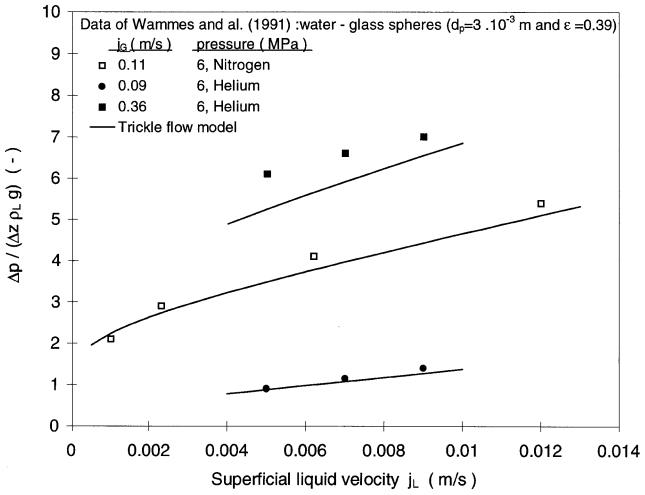

Fig. 4. Dimensionless pressure gradient vs the superficial liquid velocity in the conditions of gas–liquid trickle flow: comparison of the theoretical predictions from the trickle flow model with the experimental results of Wammes et al. (1991b).

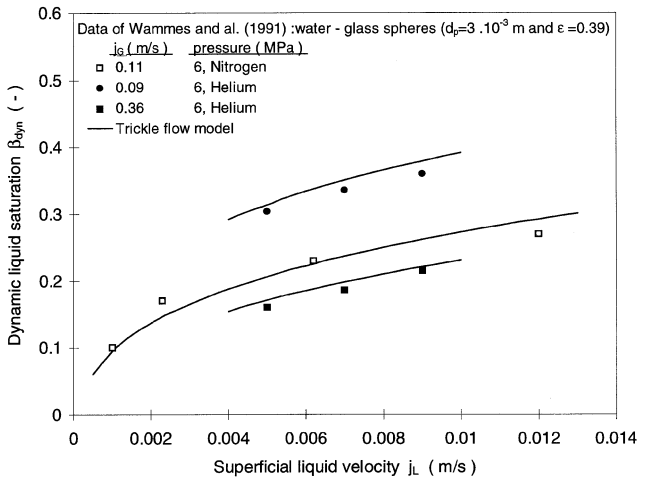

Fig. 5. Dynamic liquid saturation vs the superficial liquid velocity in the conditions of gas–liquid trickle flow: comparison of the theoretical predictions from the trickle flow model with the experimental results of Wammes et al. (1991b).

at a given gas density the liquid saturation increases with superficial liquid velocity and decreases when the superficial gas velocity increases. At given superficial velocities it decreases when the gas density increases.

The great influence of the gas flow, via the density or/and the superficial gas velocity, is well predicted from the theoretical model and is essentially attributed to variations of the momentum fluxes corresponding to both gas flow ($\rho_G j_G^2$) and gas–liquid slip motion ($\rho_G j_r^2$). The increase of these quantities leads to a non-negligible rise of the mechanical energy dissipation resulting from the liquid-side shear stress at the gas–liquid interface which becomes of great importance compared to the other momentum transfer mechanisms (liquid–solid drag and gravity forces). Accordingly, the resulting increase of interaction forces exerted on the liquid film by the gas flow leads to a significant rise of pressure gradient (Fig. 4) as well as a reduction of the mean residence time of liquid in the reactor, and thus a significant decrease of liquid saturation (Fig. 5). It can be seen in Fig. 4 that the theoretical results from the present model underestimate the pressure gradient at high operating pressures and superficial gas velocities. In these conditions, a question arises about the stability of the liquid film due to the important shear stress exerted by the gas flow. Generally, the numerical results are in good agreement with the experimental data of Wammes et al. (1990,1991a–c): the relative errors are less than 40 and 15%, respectively, for the pressure gradient and liquid saturation.

Larachi et al. (1991) have presented measurements of pressure gradient and total liquid saturation for cocurrent gas–liquid downward flows through packed beds of glass beads (diameter either 1.4 or 2 mm) in the range of operating pressure 0.2–8.1 MPa. These experiments have been performed in the trickle flow regime, trickle-pulsed flow transition and pulsed-flow regime. The diagram of Charpentier and Favier (1975), modified by Larachi (1991) in order to take into account the effect of the operating pressure, has been used to isolate the experimental points obtained in the trickle flow regime. The predictions of the trickle flow model are compared with experimental results of Larachi et al. in Figs. 6–8 for pressure gradient and Figs. 9 and 10 for dynamic liquid saturation. The theoretical model is able to predict quite well the significant influence of the gas flow on the hydrodynamic parameters. At given mass flow rates, the pressure gradient decreases when the gas density increases (Fig. 6) and the opposed trend is predicted for the liquid saturation (Fig. 9). These effects are essentially attributed to the decrease of the momentum fluxes corresponding to both gas flow ($\rho_G j_G^2 = G_G^2/\rho_G$) and gas–liquid slip motion.

Comparing in Fig. 7 the results of pressure gradient obtained for both diameters of tested particles, it can be seen that the theoretical predictions from the model exhibit a better accuracy when the particle diameter is

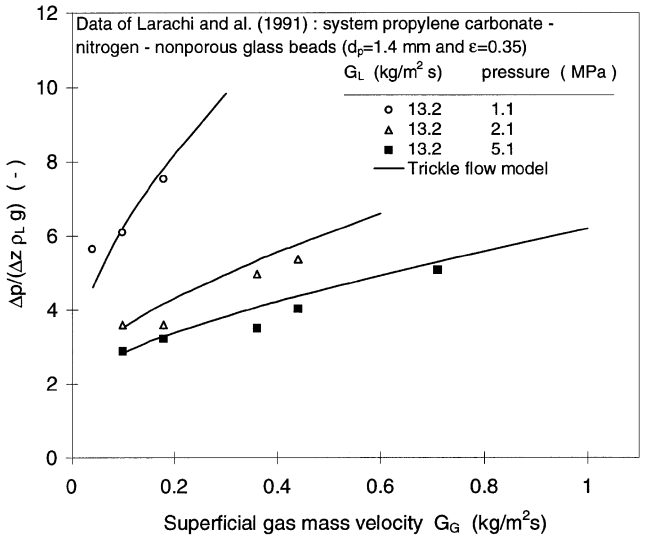

Fig. 6. Dimensionless pressure gradient vs the superficial gas mass velocity: comparison of the theoretical predictions from the trickle flow model with the experimental results of Larachi et al. (1991), influence of the operating pressure.

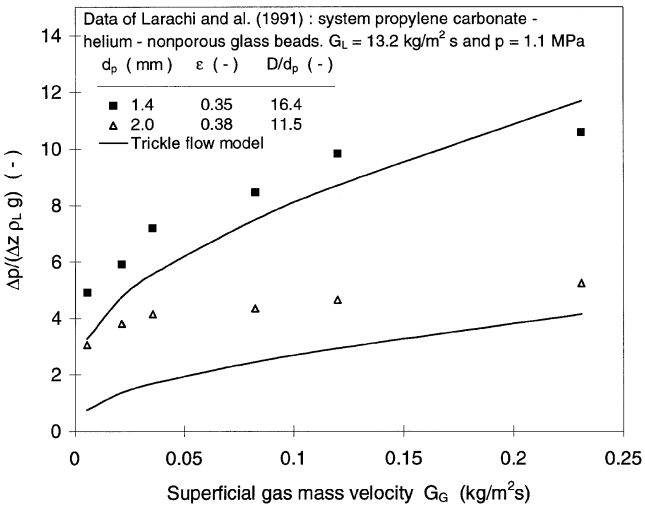

Fig. 7. Dimensionless pressure gradient vs the superficial gas mass velocity: comparison of the theoretical predictions with the experimental results of Larachi et al. (1991a, b), influence of the particles diameter.

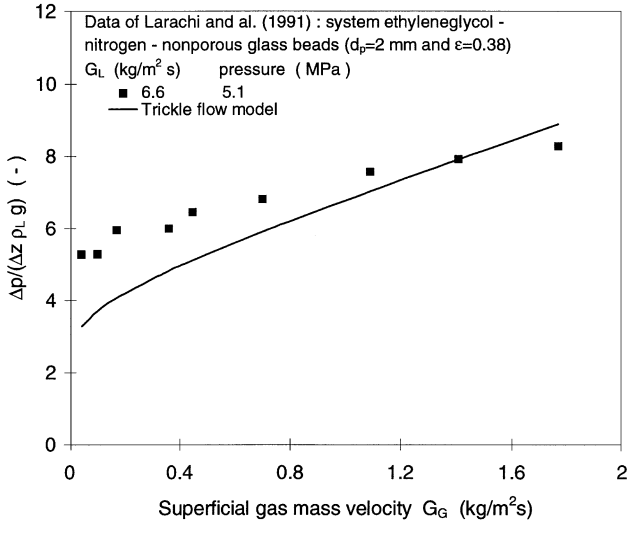

Fig. 8. Dimensionless pressure gradient vs the superficial gas mass velocity: comparison of the theoretical predictions with the experimental results of Larachi et al. (1991a, b), influence of the gas mass flow rate.

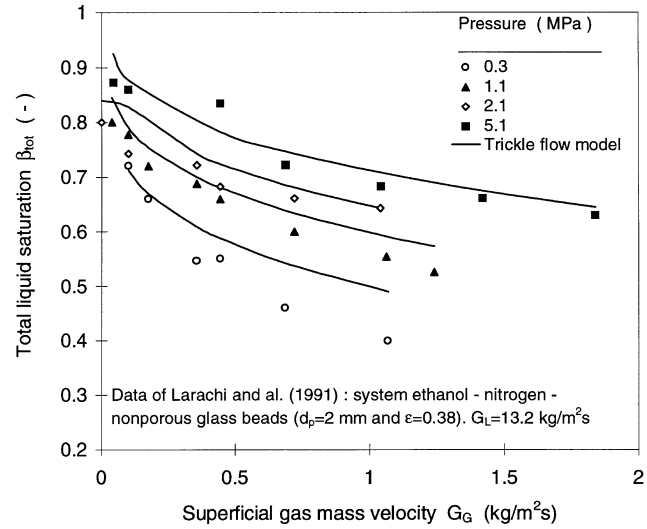

Fig. 9. Total liquid saturation vs the superficial gas mass velocity: comparison of the theoretical predictions from the trickle flow model with the experimental results of Larachi et al. (1991a, b), influence of the operating pressure.

1.4 mm than when the particle diameter is 2 mm. The discrepancy observed for the greater diameter is attributed to the wall column effect which arises when the ratio of column diameter over particles diameter D/d_p becomes small enough as evoked by several authors (Specchia et al., 1974; Baldi and Specchia, 1976; Herskowitz and Smith, 1978). Indeed, it is usually admitted in the literature that, for all hydrodynamic regimes, the radial distribution of liquid flow can be considered as uniform over the cross-sectional area of the reactor when the value of the ratio D/d_p is less than some critical value. This critical value varies from one author to another: Baker et al. (1935) have proposed a minimum value of 12, Herskowitz and Smith (1978) have suggested 18 and Al-Dahhan and Dudukovic (1994) have reported that a value of D/d_p greater than 20 minimises the nonuniformity of liquid flow. In the experiments of Larachi et al. (1991a, b), the particles of 2 mm diameter correspond to a value of D/d_p equal to 11.5 which is smaller than all critical values evoked in the literature. Accordingly, in

the packed bed involving particles of 2 mm diameter, the liquid flow exhibits preferential paths near the column wall where the local porosity is higher. This two-dimensional phenomenon is not taken into account by the present 1-D model. Additionally, at higher gas mass flow rates, the theoretical results of pressure gradient come closer to the experimental data for the packed bed involving particles of 2 mm (Figs. 7 and 8). Indeed, the increase of the gas mass flow rate produces more important interactions between the fluids improving the uniform distribution of liquid flow over the whole cross-sectional area of the reactor. As a matter of fact, this result of theoretical predictions agrees with the experimental tendency which has shown a reduction of liquid flow rate near the wall column when the gas flow rate increases (Baldi, 1981).

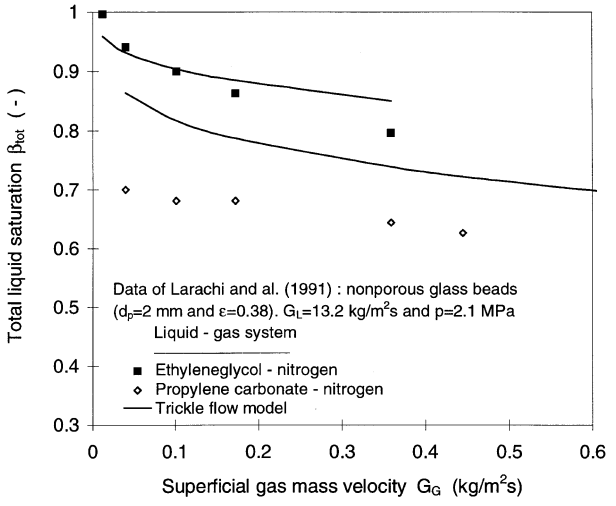

Fig. 10. Total liquid saturation vs the superficial gas mass velocity: comparison of the theoretical predictions with the experimental results of Larachi et al. (1991a, b), influence of the nature of the liquid.

The predictions of liquid saturation from the present model overestimate systematically the experimental results of Larachi et al. (1991a, b) especially for the packed bed with particles of 2 mm diameter (Figs. 9 and 10). This overestimation is attributed to the above mentioned wall channelling which reduces significantly the mean residence time of liquid in the reactor. By comparing in Fig. 10 the results obtained at elevated liquid mass velocity $G_L = 13.2$ kg/m^2 s for ethyleneglycol and propylene carbonate, it can be seen that the liquid saturation is more overestimated by the theoretical predictions in the case of propylene carbonate compared to the case of ethyleneglycol. In fact, propylene carbonate is a liquid which exhibits a weakly foaming behaviour at high liquid mass flow rates. Probably, the high stability of fine bubbles to set on the packing surface when the liquid foams leads to a lower value of liquid saturation in foaming systems. Generally, the numerical results are in good agreement with the experimental data of Larachi (1991), Larachi et al. (1991a, b): the relative errors are less than 45 and 20% for the pressure gradient and liquid saturation, respectively.

Al-Dahhan and Dudukovic (1994) have performed measurements of pressure gradient and total liquid saturation for cocurrent gas–liquid trickle flow through packed beds of glass beads, porous spherical silica and porous extrudates in the range of operating pressure 0.31–5 MPa. The theoretical predictions from the trickle flow model are compared with experimental results of Al-Dahhan and Dudukovic in Figs. 11–13 for pressure gradient and Figs. 14 and 15 for total liquid saturation. In these figures, comparisons with the predictions from the model of Holub et al. (1992, 1993) are also presented. The values of the two parameters of this model are given for each packed bed by Al-Dahhan and Dudukovic (1994) from experiments performed in single-phase flow. The predictions of the present model are more accurate

Table 2
High-pressure experimenatal data examined

Authors	Systems	Operating conditions
Wammes et al. (1990, 1991a–c)	Water, ethanol, 40% ethyleneglycol, nitrogen, helium Glass spheres: 3 mm Ceramic cylinders: 3.2 × 3.2 mm $15.9 < D/d_p < 17$	Pressure: 0.2–7.5 MPa j_L max. = 1.6 cm/s j_G max. = 36 cm/s
Larachi et al. (1991a, b)	Water, ethanol, propylene carbonate, ethyleneglycol, water + 40% sucrose, water + 1% ethanolnitrogene, helium, argon Glass beads: 1.4; 2 mm $11.5 < D/d_p < 16.4$	Pressure: 0.2–8.1 MPa G_L: 1.8–24.5 kg/m^2 s G_G: 0.003–3 kg/m^2 s
Al-Dahhan and Dudukovic (1994)	Water, hexane, nitrogen, helium Glass spheres: 1.14 mm Silica shell spheres: 1.52 mm 0.5% Pd/alumina extrudates: 1.99 mm $11 < D/d_p < 20$	Pressure: 0.31–5 MPa G_L: 0.42–4.1 kg/m^2 s G_G: 6.64×10^{-3}–4.03 kg/m^2 s

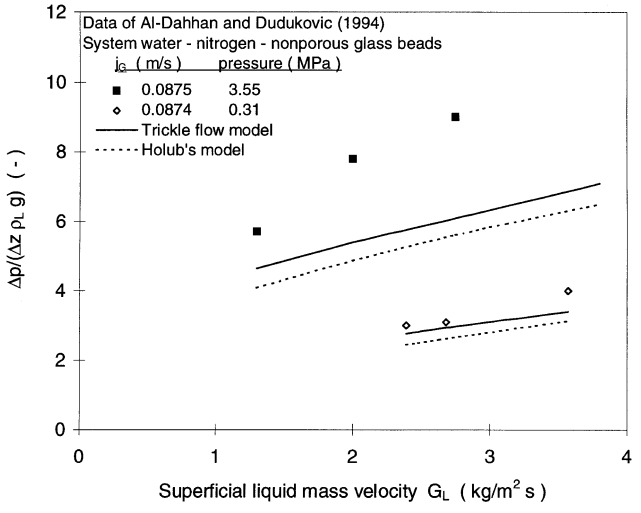

Fig. 11. Dimensionless pressure gradient vs the superficial liquid mass velocity: comparison of the theoretical predictions with the experimental results of Al-Dahhan and Dudukovic (1994), non-porous glass beads.

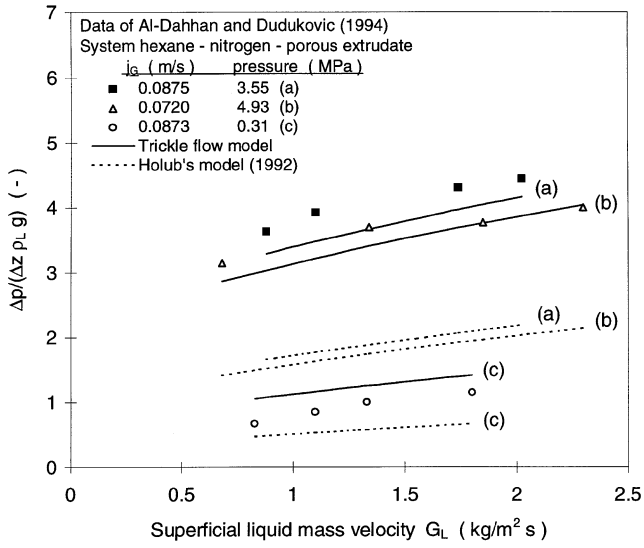

Fig. 13. Dimensionless pressure gradient vs the superficial liquid mass velocity: comparison of the theoretical predictions with the experimental results of Al-Dahhan and Dudukovic (1994), porous extrudates.

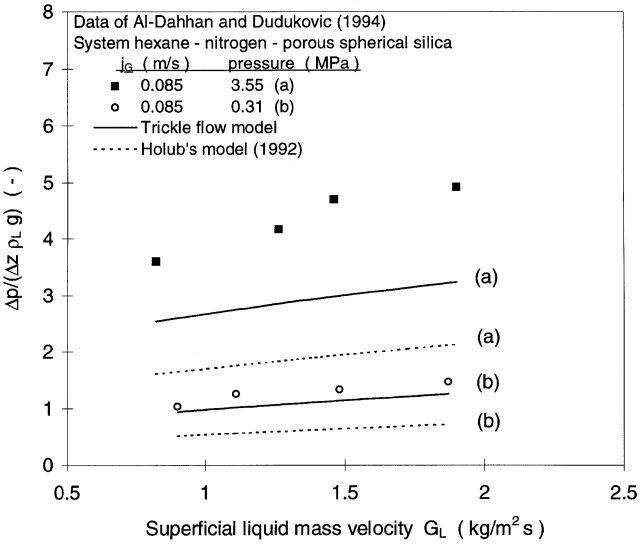

Fig. 12. Dimensionless pressure gradient vs the superficial liquid mass velocity: comparison of the theoretical predictions with the experimental results of Al-Dahhan and Dudukovic (1994), porous spherical silica.

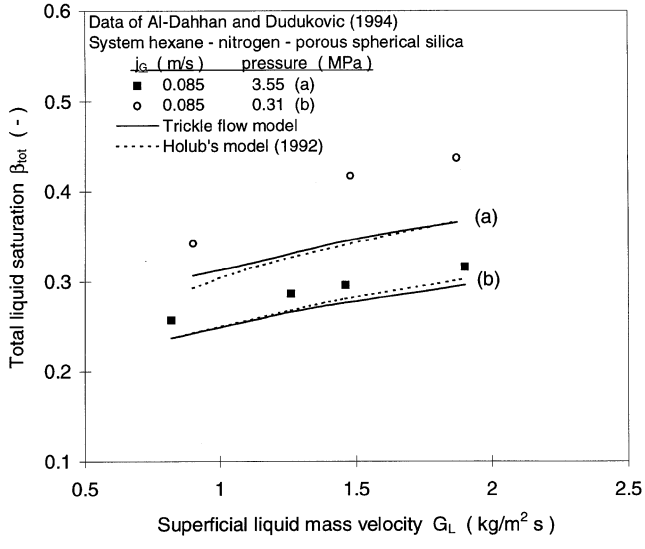

Fig. 14. Total liquid saturation vs the superficial liquid mass velocity: comparison of the theoretical predictions with the experimental results of Al-Dahhan and Dudukovic (1994), porous spherical silica.

than the ones given from the model of Holub et al. in the whole range of operating conditions investigated by the authors. This improvement can be explained by the fact that, as opposed to the model of Holub et al. in which the parameters of gas–liquid interaction are taken as zero, in the present analysis the formulation of balance equations has a fundamental basis and the mutual fluids interactions are taken into consideration. However the values of liquid saturation predicted from both models are close (Figs. 14 and 15).

It can be seen that the theoretical results from the present model underestimate systematically the pressure gradient at high operating pressures and superficial gas velocities (Figs. 11–13, for $j_G = 0.0875$ m/s and $p = 3.55$ MPa). A similar trend has been noted by comparing the calculated pressure gradient from the present model and the data of Wammes et al. (1991b) (Fig. 3, for $j_G = 0.11$ m/s and $p = 6$ MPa/N_2). In these conditions, the liquid-side shear stress exerted by the gas flow at the fluids interface becomes of great importance due to the

high inertia of the gas phase. The strong drag exerted by the gas flow is responsible for the loss of laminar liquid film stability. As a consequence, the gas–liquid interface exhibits a roll waves and ripples pattern which corresponds to an increase of roughness with respect to smooth gas–liquid interface conditions. Furthermore, at high gas mass flow rates, the gas inertia becomes high enough to balance the surface tension forces of liquid and, as a consequence, some dispersed droplets can be drained by the turbulent gas flow down the reactor. The droplets entrainment phenomenon is another process of the mechanical energy dissipation. Since the effective interfacial roughness as well as the droplets entrainment process are not taken into account by the present model, the theoretical predictions of pressure gradient will be systematically less than the actual values in the conditions of high operating pressures and superficial gas velocities. However, in these conditions, the error of predictions from the present model is not more than the inaccuracy of the literature correlations. Generally, the theoretical predictions from the present model are in good agreement with the experimental results of Al-Dahhan and Dudukovic (1994): the relative errors are less than 40 and 15% for, respectively, the pressure gradient and liquid saturation.

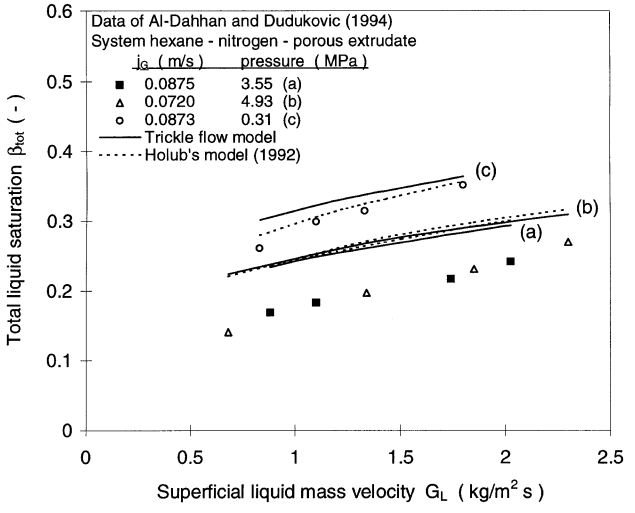

Fig. 15. Total liquid saturation vs the superficial liquid mass velocity: comparison of the theoretical predictions with the experimental results of Al-Dahhan and Dudukovic (1994), porous extrudates.

7.3. Comparisons of the trickle flow model and available correlations predictions with experimental data

The available correlations for the predictions of pressure gradient and liquid saturation, validated in a wide range of operating pressure, are presented in Table 1. The mean relative error $\langle e_\Psi \rangle$ between the predicted and experimental values of the hydrodynamic parameter Ψ (pressure gradient or liquid saturation) is calculated from

$$\langle e_\Psi \rangle = \frac{1}{N} \sum_{i=1}^{N} \frac{|\Psi_{\text{predicted}} - \Psi_{\text{experimental}}|}{\Psi_{\text{experimental}}}$$

where N is the number of data points. The deviation of the relative error around the mean value $\langle e_\Psi \rangle$ is evaluated from the mean quadratic deviation defined as the square root of the quadratic variance:

$$\sigma_\Psi = \left(\sum_{i=1}^{N} \frac{(\langle e_\Psi \rangle - e_\Psi)^2}{N} \right)^{1/2}.$$

The results of mean relative errors and quadratic deviations obtained by comparing the theoretical results of each correlation and models with the experimental data sets of Wammes et al. (1990, 1991a–c), Larachi et al. (1991a, b) and Al-Dahhan and Dudukovic (1994) are, respectively, presented in Tables 3–5. Furthermore, the statistical parameters $\langle e_\Psi \rangle$ and σ_Ψ are also calculated by comparing the theoretical results of each correlation and models with the set of all experimental data examined in this work. Such results are summarised in Table 6.

It can be seen in Tables 3–5 that the predictions of pressure gradient and liquid saturation from each correlation are not satisfactory when they are compared with experimental results different from the data set used for the establishment of this correlation. In consequence, each correlation may become very inaccurate when it is applied to predict the hydrodynamic parameters of industrial trickle-bed reactors. On the other hand, the

Table 3
Comparison of models predictions with experimental data of Wammes et al. (1990, 1991a–c) in terms of statistical parameters $\langle e_\psi \rangle$ and σ_ψ

Statistical parameters (1991b, c)	Wammes et al. (1988, 1990)	Ellman et al. (1991a, b)	Larachi et al. (1992)	Holub et al. flow model	Trickle flow model
Pressure gradient					
$\langle e_{dp/dz} \rangle$	0.242	0.402	1.870	0.639	0.256
$\sigma_{dp/dz}$	0.288	0.238	3.452	0.147	0.228
Liquid saturation					
$\langle e_\beta \rangle$	0.070	0.231	0.207	0.130	0.107
σ_β	0.062	0.159	0.170	0.107	0.077

Table 4
Comparison of models predictions with experimental data of Larachi et al. (1991) in terms of statistical parameters $\langle e_\psi \rangle$ and σ_ψ

Statistical parameters (1991b, c)	Wammes et al. (1988, 1990)	Ellman et al. (1991a, b)	Larachi et al. (1992)	Holub et al. flow model	Trickle flow model
Pressure gradient					
$\langle e_{dp/dz} \rangle$	0.395	0.845	0.208	0.547	0.307
$\sigma_{dp/dz}$	0.219	0.117	0.252	0.176	0.193
Liquid saturation					
$\langle e_\beta \rangle$	0.157	0.154	0.072	0.147	0.144
σ_β	0.082	0.168	0.084	0.081	0.090

Table 5
Comparison of models predictions with experimental data of Al-Dahhan and Dudukovic (1994) in terms of statistical parameters $\langle e_\psi \rangle$ and σ_ψ

Statistical parameters (1991b, c)	Wammes et al. (1988, 1990)	Ellman et al. (1991a, b)	Larachi et al. (1992)	Holub et al. flow model	Trickle flow model
Pressure gradient					
$\langle e_{dp/dz} \rangle$	0.824	0.603	1.655	0.452	0.254
$\sigma_{dp/dz}$	0.340	0.239	1.287	0.231	0.171
Liquid saturation					
$\langle e_\beta \rangle$	0.531	0.215	0.201	0.102	0.126
σ_β	0.075	0.162	0.150	0.094	0.095

Table 6
Comparison of models predictions to the set of experimental data in terms of statistical parameters $\langle e_\psi \rangle$ and σ_ψ

Statistical parameters (1991b, c)	Wammes et al. (1988, 1990)	Ellman et al. (1991a, b)	Larachi et al. (1992)	Holub et al. flow model	Trickle flow model
Pressure gradient					
$\langle e_{dp/dz} \rangle$	0.524	0.648	0.766	0.530	0.275
$\sigma_{dp/dz}$	0.311	0.220	1.782	0.209	0.195
Liquid saturation					
$\langle e_\beta \rangle$	0.230	0.334	0.272	0.132	0.121
σ_β	0.203	0.581	0.507	0.097	0.088

present model predicts the pressure gradient and liquid saturation with a respective accuracy nearly constant when its theoretical results are compared with the various data sets. As a matter of fact, the present model shows no dependence with regard to a particular experimental data set. The mean relative errors in pressure gradient and liquid saturation for the present model, respectively, are 27.5 and 12.1% (Table 6). They are smaller than the respective mean relative errors obtained with the available high-pressure correlations. The accuracy of liquid saturation predictions from the trickle flow model is close to the one expected by the model of Holub et al. (1992). However, contrary to the model of Holub et al., the present approach does not involve any parameter to fit experimental data. The parity plots presented in Figs. 16 and 17 compare, respectively, the pressure gradient and liquid saturation calculated from the proposed model with all experimental data examined in this work.

The reason for the significant improvement of the proposed approach might be, as opposed to the available correlations, that the present model is based on a formulation deduced from the fundamental macroscopic balance laws as well as a physical description of the various interactions phenomena in a multiphase catalytic reactor. The resulting model (14), based on an idealised picture of the trickle flow regime, does not require any parameter from fitting of two-phase or single-phase flow data where several phenomena could be encountered simultaneously (radial non uniformity of the liquid flow, column wall effects, foaming phenomenon, axial dispersion, droplets entrainment, etc.). This is essentially the reason why, contrary to the correlations with adjustment parameters, the relative discrepancy observed in specific

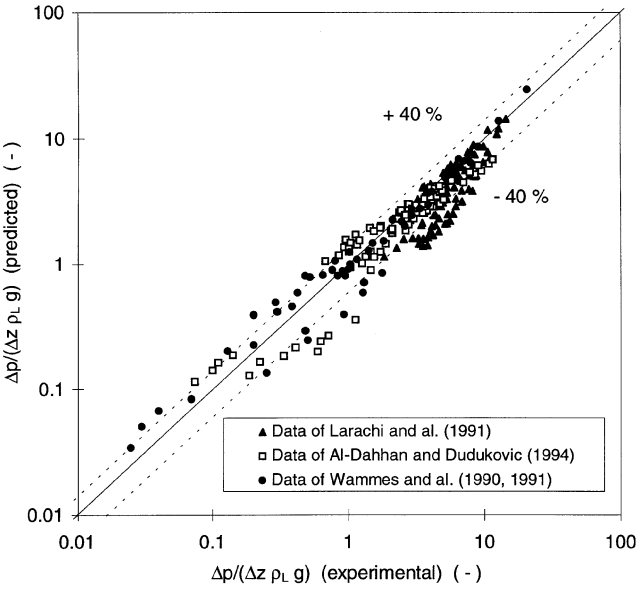

Fig. 16. Parity plot for the prediction of the pressure gradient using the trickle flow model (14).

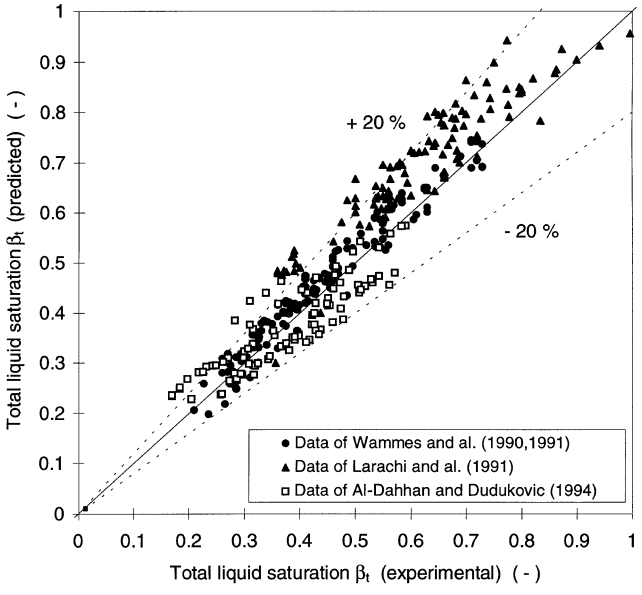

Fig. 17. Parity plot for the prediction of the liquid saturation using the trickle flow model (14).

conditions between the predictions from the proposed model and the experimental results could be interpreted on the basis of physical arguments.

8. Discussion and conclusions

Analysis of the hydrodynamic behaviour of the cocurrent gas–liquid trickle-bed reactors have mostly been performed with empirical corrections validated in a specific range of operating conditions and bed characteristics. The few available correlations developed in a wide range of operating pressure are not reliable to predict the hydrodynamic parameters of industrial trickle-bed reactors. Furthermore, they do not give a better understanding of physical phenomena. In this study, a physical one-dimensional model has been developed to describe the hydrodynamics of a steady-state cocurrent gas–liquid trickle flow through a trickle-bed reactor. The trickle flow regime is idealised by a flow in which the gas and liquid phases are completely separated by a smooth and stable interface. As a consequence, each fluid behaves as a continuous medium for which the macroscopic balance laws can be applied in the eulerian formalism. The formulation of the trickle flow model involves the global mass and momentum balance equations applied to each fluid flowing across the interstitial void volume. The closure equations describing the various interactions between the phases are formulated on the basis of theoretical considerations by taking into account the assumed idealised flow pattern. The resulting model (set (14)) has the fundamental characteristic to involve no parameter from fitting two-phase or single-phase flow data.

The approach developed to describe the liquid–solid interaction is validated on the basis of the good agreement between the experimental data of liquid saturation and the calculated results from the model obtained in the conditions of single-phase liquid trickle flow. In conditions of gas–liquid flow, the model correctly predicts the trends observed experimentally (effects of the gas and liquid superficial velocities, operating pressure, gas molecular weight, particles diameter and global bed porosity). A good agreement is generally observed between the predictions of pressure gradient and liquid saturation from the model and the respective experimental results obtained in a large range of operating pressure (about 0.1–10 MPa). The accuracy of the model for the predictions of the two hydrodynamic parameters is better than the available correlation ones: the mean relative errors in pressure gradient and liquid saturation are, respectively, equal to 27.5 and 12.1%.

The proposed model underestimates the pressure gradient in the conditions of high operating pressures and superficial gas velocities due to the apparition of roll waves pattern of the gas–liquid interface and the droplets entrainment phenomenon. In these conditions, the assumption of smooth and stable gas–liquid interface becomes doubtful. Additionally, the discrepancy between the theoretical predictions from the model and the experimental results decreases when the column diameter over particles diameter ratio (D/d_p) increases. This trend is attributed to the column wall effect which has been found to have a great importance for D/d_p values less than about 12–14.

The theoretical predictions from the model correctly take into consideration the strong influence of the gas flow on the hydrodynamic behaviour of trickle-bed

reactors shown by the various pertinent experiments examined in this work. The important influence of the gas flow is attributed to the interactions phenomena exerted by the gas phase on the liquid phase. These interactions clearly appear to be significant at high operating pressures, even at relatively low superficial gas velocities, and at high superficial gas velocities, even at relatively low operating pressures.

Notation

A effective cross-sectional area of the interstitial space, m^2
A_1, A_2 cross-sectional areas of the closed surface S (Fig. 1), m^2
A_i momentum transfer coefficient associated to the force by which the gas pushes the liquid film against the solid particles, m^{-2}
$A_{KK'}$ momentum transfer coefficient between phases K and K', m^{-2}
A_S solid particles area of the closed surface S (Fig. 1), m^2
B_i momentum transfer coefficient associated to the force by which the gas pushes the liquid film against the solid particles, m^{-1}
$B_{KK'}$ momentum transfer coefficient between phases K and K', m^{-1}
D reactor diameter, m
d_p particle diameter, m
f_i resultant of the force by which the gas pushes the liquid film against the solid particles per unit volume of void space of the packed bed, N/m^3
$f_{\text{int},K}$ resultant of interaction forces exerted on the K-fluid ($K = G$ or L) per unit volume of void space of the packed bed, N/m^3
$f_{KK'}$ resultant of drag forces between phases K and K' per unit volume of void space of the packed bed, N/m^3
$\mathbf{g}$ gravitational acceleration, m/s^2
G_K superficial mass velocity of K-fluid, $kg/m^2\,s$
j_K superficial velocity of K-fluid, m/s
j_r reference superficial velocity associated to the gas–liquid slip motion, m/s
$\mathbf{n}$ unit vector normal to S, oriented towards the outside of volume V
$\mathbf{n}_K$ unit vector normal to S_i, oriented outwards with regard to the K-fluid
p pressure
R constant of ideal gas, J/kg K
Re_L dimensionless Reynolds number for the liquid defined by $\rho_L j_L d_p/\mu_L$
S closed surface bounding the interstitial control volume V (Fig. 1), m^2
S_i gas–liquid interface area, m^2
T temperature, K
$\mathbf{T}_K$ total stress tensor of the K-fluid, Pa
u_K average interstitial velocity of the K-fluid, m/s
V control volume of the interstitial void space in the packed bed (Fig. 1), m^3
$\mathbf{v}_i$ interface velocity, m/s
$\mathbf{v}_K$ velocity vector of the K-fluid, m/s
X_K characteristic presence function of the K-fluid (0 or 1)
z axial coordinate, m
$\langle e_\Psi \rangle$ mean relative error for the predictions of the hydrodynamic parameter Ψ
$\mathbf{1}_z$ unit vector in the axial direction

Greek letters

α mean fraction of the interstitial void volume occupied by the gas phase
β_{dyn} dynamic liquid saturation (liquid volume per unit void volume)
β_{stat} static liquid saturation
β_{tot} total liquid saturation
Γ_K shape factor for the momentum flux of the K-fluid
ε global bed porosity
μ_K dynamic viscosity of the K-fluid, Pa s
ρ_K density of the K-fluid, kg/m^3
θ_L average tortuous pattern factor of the liquid flow path
$\boldsymbol{\tau}_K$ viscous stress tensor of the K-fluid, Pa
τ_i shear stress of the material gas–liquid (or liquid–solid) interface, Pa
σ_Ψ mean quadratic deviation for the predictions of the hydrodynamic parameter Ψ

Subscripts

G gas phase
i gas–liquid interface
int interaction
K K-fluid (gas or liquid)
L liquid phase
S solid phase
1, 2 upstream and downstream geometrical cross-sections, respectively (Fig. 1)

References

Al-Dahhan, M.H., & Dudukovic, M.P. (1994). Pressure drop and liquid holdup in high pressure trickle-bed reactors. *Chem. Engng Sci.*, *49*, 5681–5698.

Al-Dahhan, M.H., Larachi, F., Dudukovic, M.P., & Laurent, A. (1997). High-pressure trickle-bed reactors: a review. *Ind. Engng Chem. Res.*, *36*, 3292–3314.

Baker, T., Chilton, T.H., & Vernon, H.C. (1935). The course of liquid flow in packed towers. *Trans. Am. Inst. Chem. Engrs*, *31*, 296.

Baldi, G., & Specchia, V. (1976). Distribution and radial spread of liquid in packed towers with two-phase cocurrent flow: effect of packing shape and size. *Ing. Chim. Ital.*, *12*, 107–111.

Baldi, G. (1981). Hydrodynamics of multiphase reactors. In A.E. Rodrigues, J.M. Calo, & N.H. Sweed (Eds.), *Multiphase chemical reactors*, *Design methods*, (Vol. II, pp. 271–305). NATO Adv. Study Inst. Series E, Applied Sciences, No. 52. Sitjhoff and Noozdhoff, Áalphen aan den Rijn, The Netherlands.

Charpentier, J.C., & Favier, M. (1975). Some liquid holdup experimental data in trickle-bed reactors for foaming and nonfoaming hydrocarbons. *A.I.Ch.E. J*., *21*, 1213–1218.

Dankworth, D.C., Kevrekidis, I.G., Sundaresan, S. (1990). Dynamics of pulsing flow in trickle beds. *A.I.Ch.E. J*., *36*, 605–621.

Ellman, M.J., Midoux, N., Laurent, A., & Charpentier, J.C. (1988). A new improved pressure drop correlation for trickle-bed reactors. *Chem. Engng Sci*., *43*, 2201–2206.

Ellman, M.J., Midoux, N., Wild, G., Laurent, A., & Charpentier, J.C., (1991). A new improved liquid hold-up correlation for trickle-bed reactors. *Chem. Engng Sci*., *45*, 1677–1684.

Gianetto, A., & Specchia, V. (1992). Trickle-bed reactors: state of the art and perspectives. *Chem. Engng Sci*., *47*, 3197–3213.

Gianetto, A., Specchia, V., & Baldi, G. (1973). Absorption in packed towers with cocurrent downward high-velocity flows. Part II: Mass transfer. *A.I.Ch.E. J*., *19*, 916–922.

Grosser, K., Carbonell, R. G., & Sundaresan, S. (1988). Onset of pulsing in two-phase cocurrent downflow through a packed bed. *A.I.Ch.E. J*., *34*, 1850–1860.

Hanratty, T.J. (1983). Interfacial instabilities caused by air flow. In R.E. Meyer, (Ed.), *Waves on fluid interfaces*. pp. 221–259, New York: Academic Press.

Hasseni, W., Laurent, A., Midoux, N., & Charpentier, J.C. (1987). Hydrodynamics of a trickle bed reactor operating under pressure (0–10 MPa): flow regimes and pressure drop. *CHISA* '87 Session 17: Gas–Liquid Packed Bed, Prague.

Herskowitz, M., & Smith, J.M. (1978). Liquid distribution in trickle-bed reactor. Part I. Flow measurements. *A.I.Ch.E. J*., *24*, 439–450.

Holub, R.A., Dudukovic, M.P., & Ramachandran, P.A. (1992). A phenomenological model for pressure drop, liquid holdup, and flow regime transition in gas–liquid trickle flow. *Chem. Engng Sci*., *47*, 2343–2348.

Holub, R.A., Dudukovic, M.P., & Ramachandran, P.A. (1993). Pressure drop, liquid holdup, and flow regime transition in trickle flow. *A.I.Ch.E. J*., *39*, 302–321.

Ishii, M. (1975). *Thermo-fluid dynamic theory of two-phase flow*. Paris: Eyrolles.

Larachi, F. (1991). *Les réacteurs triphasiques à lit fixe à écoulement à co-courant vers le bas et vers le haut de gaz et de liquide. Etude de l'influence de la pression sur l'hydrodynamique et le transfert de matière gaz–liquide*. Ph.D. Dissertation, Institut National Polytechnique de Lorraine, Nancy.

Larachi, F., Laurent, A., Midoux, N., & Wild, G. (1991a). Experimental study of a trickle-bed reactor operating at high pressure: two-phase pressure drop and liquid saturation. *Chem. Engng Sci*., *46*, 1233–1246.

Larachi, F., Laurent, A., Wild, G., & Midoux, N. (1991b). Some experimental liquid saturation results in fixed-bed reactors operated under elevated pressure in cocurrent upflow and downflow of the gas and the liquid. *Ind. Engng Chem. Res*., *30*, 2404–2410.

Malamatenios, Ch., Giannakoglou, C., & Papailiou, K.D. (1994). A coupled two-phase shear layer/liquid film calculation method. Formulation of the physical problem and solution algorithm. *Int. J. Mult. Flow*, *20*, 593–612.

McDonald, L.F., El-Sayed, M.S., Mow, K., & Dullien, F.A.L. (1979). Flow through porous media – the Ergun equation revisited. *Ind. Eng. Chem. Fundam*., *18*, 199–208.

Ng, K.M., & Chu, C.F. (1987). Trickle-bed reactors. *Chem. Engng Progr*., *83*, 55–63.

Ng, K.M. (1986). A model for regime transitions in cocurrent downflow trickle-bed reactors. *A.I.Ch.E. J*., *32*, 115–122.

Rao, V.G., & Drinkenburg, A.A.H. (1985). A model for pressure drop in two-phase gas–liquid downflow through packed columns. *A.I.Ch.E. J*., *31*, 1010–1017.

Saez, A.E., & Carbonell, R.G. (1985). Hydrodynamic parameters for gas–liquid cocurrent flow in packed beds. *A.I.Ch.E. J*., *31*, 52–62.

Sai, P.S.T., & Varma, Y.B.G. (1987). Pressure drop in gas–liquid downflow through packed beds. *A.I.Ch.E. J*., *33*, 2027–2036.

Saroha, A.K., & Nigam, K.D.P. (1996). Trickle bed reactors. *Rev. Chem. Engng 12*, 207–347.

Satterfield, C.N. (1975). Trickle bed reactors. *A.I.Ch.E. J*., *21*, 209–228.

Specchia, V., & Baldi, G. (1977). Pressure drop and liquid holdup for two phase concurrent flow in packed beds. *Chem. Engng Sci*., *32*, 515–523.

Specchia, V., Rossini, A., & Baldi, G. (1974). Distribution an radial spread of liquid in two-phase concurrent flows in a packed bed. *Ing. Chim. Ital*., *10*, 171–176.

Sweeney, D.E. (1967). A correlation for pressure drop in two-phase cocurrent flow in packed beds. *A.I.Ch.E. J*., *13*, 663–669.

Tosun, G. (1984). A study of cocurrent downflow of nonfoaming gas–liquid systems in a packed bed. 2. Pressure drop: Search for a correlation. *Ind. Engng Chem. Process Des. Dev*., *23*, 35–39.

Wammes, W.J.A., & Westerterp, K.R. (1990). The influence of the reactor pressure on the hydrodynamics in a cocurrent gas–liquid trickle-bed reactor. *Chem. Engng Sci*., *45*, 2247–2254.

Wammes, W.J.A., Mechielsen, S.J., & Westerterp, K.R. (1991(a)). The influence of pressure on the liquid hold-up in a cocurrent gas–liquid trickle-bed reactor operating at low gas velocities. *Chem. Engng Sci*., *46*, 409–417.

Wammes, W.J.A., Middelkamp, J., Huisman, W.J., deBaas, C.M., Westerterp, K.R. (1991(b)). Hydrodynamics in a cocurrent gas–liquid trickle bed at elevated pressures. *A.I.Ch.E. J*., *37*, 1849–1862.

Wammes, W.J.A., & Westerterp, K.R. (1991(c)). Hydrodynamics in a pressurized cocurrent gas–liquid trickle-bed reactor. *Chem. Engng Technol*., *14*, 406–413.